

THE SURFACE NECKING FORMING MECHANISM IN AN AA6016 AUTOMOTIVE SHEET DURING BENDING

Q. ZHANG¹, P.Z. ZHAO^{1,2}, J.D. LIU¹, Y.J. FENG¹

¹CHINALCO Research Institute of Science and Technology, No.62, Xizhimen North Street, Beijing, 100082, China

²Suzhou Research Institute for Nonferrous Metals, No.200, Dongshenhu Road, Suzhou, 215026, China

Keywords: AA6016, automotive sheet, necking, anisotropy, shear band, crystallographic texture

Abstract

The microstructures and the bending performance in rolling direction (RD) and transverse direction (TD) of an AA6016-T4P automotive sheet were investigated. The surface necking forming mechanism together with the initiation and propagation of shear bands during bending were studied in detail. The results indicated that no macro-crack formed in both RD and TD specimens after 180° bending, but RD specimen exhibited inferior bendability compared with TD specimen, showing more severe surface necking. The anisotropy of surface necking in the AA6016-T4P sheet was caused by special crystallographic texture, rather than grain shape and spatial distribution of the constitute particles. The total volume fraction of Goss_{ND90}, R, P, and Cu orientations was almost twice as that of Goss orientation in the AA6016-T4P sheet, resulting in the facilitation of the initiation and propagation of shear bands in the RD specimens. Two bundles of shear bands intersected at the surface where strain localized, forming the surface necking, so RD direction had more severe surface necking than TD direction.

Introduction

The demanding of weight reduction in automotive body is increasing the applications of aluminum automotive sheets so as to increase fuel efficiency and reduce vehicle emissions [1-3]. Heat-treatable 6xxx series alloys (Al-Mg-Si alloys) are generally used as automotive body outer panels because of their high paint bake response and their comparatively good formability [4,5]. For the outer panel, the bendability is very important, because it is joined with inner panels by hemming (180° bending) [6]. Previous studies indicated that the bendability of aluminum alloy sheets depended on several factors, such as solute elements [7], second phase particles [8], grain size [9], crystallographic texture [10,11], etc., and is usually anisotropic [8-11].

Takeda et al. [10] studied the correlation between crystal orientation and bendability in an Al-Mg-Si alloy sheet, and found that <001>_{ND}-orientation specimens exhibited the highest degree of bendability and the lowest anisotropy among all types of crystal directions due to the inhibition of shear bands. Ikawa et al. [11] and Kuroda et al. [12] investigated the effects of crystal orientation on the bendability in 6061-T4 alloy sheets by experiments and finite element simulation, showing that the specimens with cube texture exhibited the excellent bendability regardless of the bending direction, meanwhile, the bendability of the specimens with Goss texture strongly depended on the bending direction. However, the studies of Takeda et al. [10] and Ikawa et al. [11] were conducted based on single crystal specimens. The situation for the poly-crystal materials has not yet been made clearly.

The studied results of Davidkov et al. [9] also showed that 6016 aluminum alloy sheets developed as automotive body outer panels had better bendability as the bending line was aligned with rolling line (RD), however, the mechanism account for the fact were not revealed in this literature. Shi et al. [13] found that the anisotropy of bendability in a 6xxx alloy sheet clad with AA3003 alloy increased with the increase of the pre-strain, but the authors did not give the reason for this phenomenon. For AA7108 rolled and recrystallized aluminum alloy sheets, Westerman et al. [8] suggested that the anisotropy of bendability should be attributed to the alignment of constitute particles along the deformation direction.

The bendability of 6xxx aluminum sheets are characterized by minimum bending radius without any defects on the surface. The defects were usually classified into two patterns. One is inter granular fracture and forming macro-cracks, and another is strain localization and forming surface necking. For the 6016 aluminum alloy sheets used as automotive body outer panels, both macro-crack and severe surface necking are not allowed. Mattei et al. [14] suggested that there was a close relationship between surface necking and shear bands. However the authors did not clarify how the shear bands induced the surface necking, and did not study the anisotropy of necking

Based on the above analysis, although some results about the surface necking during bending were reported, the forming mechanism has not been clarified. In the present study, the bending performance in both RD and TD directions of an AA6016 alloy sheet with T4P temper (solution treatment and pre-aged) was investigated from the viewpoint of surface necking forming. The correlation between the surface necking and shear bands was studied in detail. The objective is to clarify the surface necking forming mechanism in both RD and TD directions .

Experimental procedures

AA6016 alloy (0.5mass%Mg, 1.2mass%Si, 0.2mass%Fe, 0.1mass%Mn and Al bal.) was used in this study. The ingot was cast by DC. After scalping, the ingot was homogenized, hot rolled, and cold rolled to the final gauge of 0.9 mm. Then the sheets were solution treated in a continuous annealing line and pre-aged (T4P temper) in order to stabilize the microstructure and improve paint bake response during the final automotive paint baking cycles.

Bending test specimens have a 50 mm×30 mm rectangular shape with gauge of 0.9 mm. The specimens were cut from the sheets along the rolling direction (hereafter referred as RD specimens) and transverse direction (hereafter referred as TD specimens). 10% pre-strain was given by tensile before bending test. Bending tests were conducted on a custom-made device which satisfies the ASTM E290 standard [15]. During the bend test, the specimens were supported on two fixed cylinders and were bend to a certain angle by applying force with a plunger. The

bending angles are designed as 60°, 90°, 120°, 150°, 180°, respectively. The radius of the plunger is 0.5 mm.

The microstructures of the sheet were examined by optical microscopy (OM, NIKON EPIPHOT 200) and scanning electron microscopy (SEM, JEOL JSM-6480) with energy-dispersive

spectroscopy (EDS) and electron backscatter diffraction (EBSD). Shear bands were observed from the cross section of the bent specimens after aging at 175 °C for 2 hours, because they became easy to be observed by etching Mg₂Si precipitates formed on the sites of the shear bands during aging.

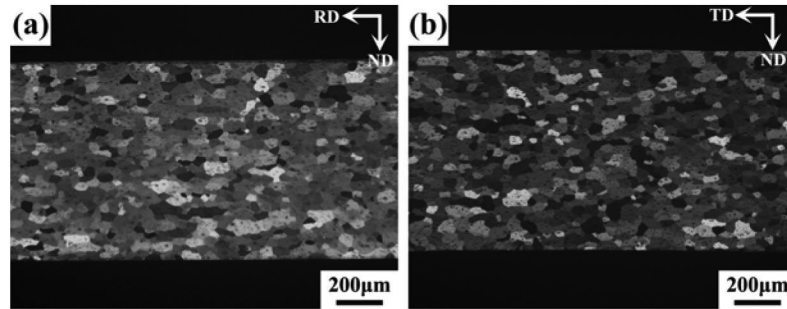


Figure 1. Through-thickness grain structure of 6016-T4P sheet in (a) RD×ND and (b) TD×ND planes

Results and Discussion

Microstructures of 6016-T4P sheets

Figure 1 shows the through-thickness grain structure of the 6016-T4P sheets. The recrystallized grains were revealed in both RD×ND and TD×ND planes, and the grain size in thickness direction is uniform. The average diameters and aspect ratios of the grains are shown in Table I. It is shown that the diameters and aspect ratios of the grains in both planes are almost same.

Figure 2 shows SEM images of the 6016-T4P sheet. The white particles which exhibit rod shape are distributed uniformly in both RD×ND and TD×ND planes. EDS results indicate that these particles are AlFeMnSi constitute phases. The average diameters and aspect ratios of the particles are similar in both two planes (Table I). The AlFeMnSi phase intermetallic compounds formed during DC casting were broken into particles by homogenization and rolling, and distributed uniformly in the sheets [16].

Table I. Average diameters and aspect ratios of the grains and constitute particles

	Grain		Constitute particle	
	Diameter, µm	Aspect ratio	Diameter, µm	Aspect ratio
RD×ND plane	44	1.46	1.09	2.72
TD×ND plane	47	1.50	1.15	2.79

Figure 3 gives the EBSD results of the 6016-T4P sheets obtained from RD×ND plane. The main texture components in the 6016-T4P sheet are Cube, Cube_{ND45}, Goss, Goss_{ND90}, R and P orientations, which is essentially similar with those in the recrystallized 6xxx alloys reported in the previous literatures [4,17]. Furthermore, some weak rolling texture components are also revealed, including Cu, S and Brass orientations. The volume fractions of the various texture components are shown in Table II.

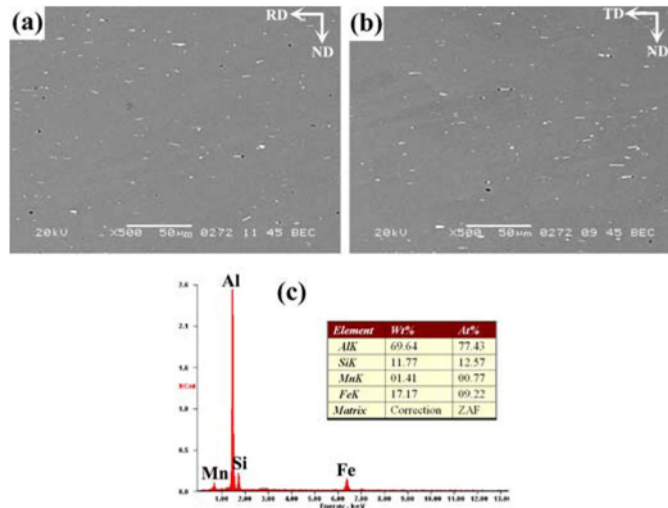


Figure 2. SEM images of 6016-T4P showing the constitute particles: (a) RD×ND plane, (b) TD×ND and (c) EDS spectra of the constitute particles

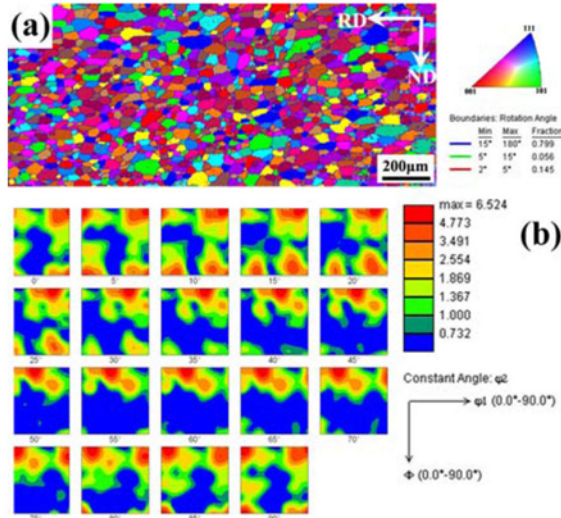


Figure 3. EBSD results of 6016-T4P sheet: (a) EBSD orientation map, and (b) ϕ_2 sections of ODFs

Table II. Volume fractions of the various texture components

Texture component	Mill indices	Volume fraction, %
Cube	{001}<100>	8.6
Cube _{ND45}	{001}<110>	0.9
Goss	{011}<100>	3.2
Goss _{ND90}	{110}<110>	2.6
R	{124}<211>	1.9
P	{011}<122>	1.6
S	{123}<634>	0.9
Brass	{011}<211>	1.7
Cu	{112}<111>	0.7

Bending performance in RD and TD directions

Figure 4(a) and (b) show the surfaces topography of the RD and TD specimens after 180° bending, no cracks are observed on the surfaces of both specimens. However, surface necking is found in both specimens, and the surface necking of RD specimen is more severe than that of TD specimens. Figure 4(c) and (d)

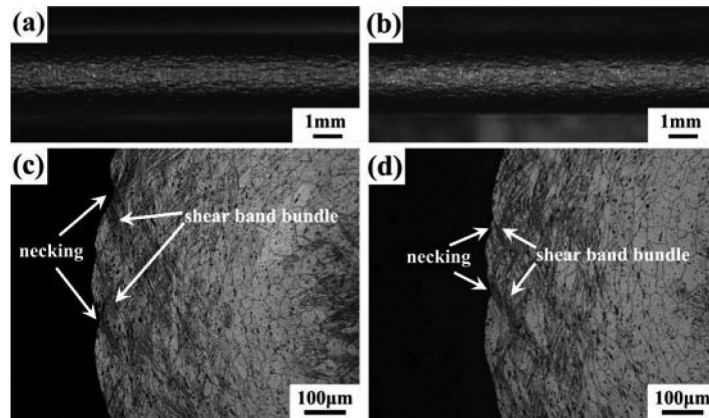


Figure 4. Bending performance of the RD and TD specimens subjected to 180° bending: (a) and (b) surface topography of the RD and TD specimens, respectively; (c) and (d) cross sections of the RD and TD specimens, respectively

show the cross sections of the RD and TD specimens after 180° bending. Some pronounced shear bands are observed in both specimens. However, the density of shear bands in RD specimen is higher than that in TD specimen.

Takeda et al. [10] had concluded that the shear band behaved as the initiation of the cracks and the propagation path. In order to investigate the forming process of surface necking and the shear bands during bending, the surface topography and the cross sections of the specimens after 60°, 90°, 120°, 150° bending were investigated in detail, and the results are shown in Figure 5 and 6, respectively.

After 60° bending, no surface necking were revealed (Figure 5(a) and (b)), and single shear band is revealed in some outer grains in RD and TD specimens were found (Figure 6(a) and (b)). In the RD specimen, as the bending angle increases to 90°, evidence surface necking is revealed (Figure 5(c)). The shear bands propagate through some grains, and some shear bands is found to be intersected at the bottom of the necking (Figure 6(c)). In the TD specimen, as the bending angle increased to 90°, obvious surface necking was still not observed (Figure 5(d)), and the density of the shear band increases, however, no intersection of shear bands was found.

With the increase of bending angle from 90° to 150° in the RD specimen, the necking of the surface became more severe (Figure 5(e)) and the density of the shear bands increased (Figure 6(e)). In the TD specimen, as the bending angle increases to 120°, the surface necking formed (Figure 5(f)) and some shear bands intersected at the bottom of the necking (Figure 6(f)). The surface necking becomes more severe and the density of the shear bands increase by increasing the bending angle from 120° to 150° in both RD and TD specimens (Figure 5(g) and (h), Figure 6(g) and (h)).

From the results of the Figure 4 and Figure 5, it can be concluded that bendability of the 6016-T4P sheets in the present study is also anisotropy, namely the surface necking of RD specimen is more sever compared with TD specimen. Previous studies [8-13] indicated that anisotropy of bendability of Aluminum alloy sheet would be attributed the following factors: (1) grain shape, (2) spatial distribution of the constitute particles, (3) crystallographic texture. The 6016-T4P sheets in the present study have the same grain shape and spatial distribution of the constitute particles in RD×ND and TD×ND planes, thus the anisotropy of necking would be caused by the crystallographic texture. And the initiation and propagation of shear bands are influenced by crystallographic texture mainly [10,11].

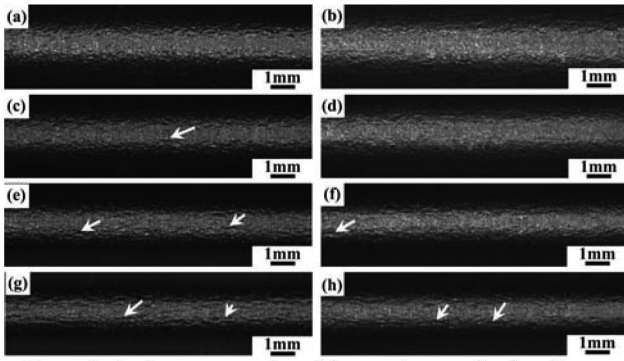


Figure 5. Surface topography of the specimens after bending to different angles: (a) RD, 60°, (b) TD, 60°, (c) RD, 90°, (d) TD, 90°, (e) RD, 120°, (f) TD, 120°, (g) RD, 150°, (h) TD, 150° (the surface necking was indicated by white arrows)

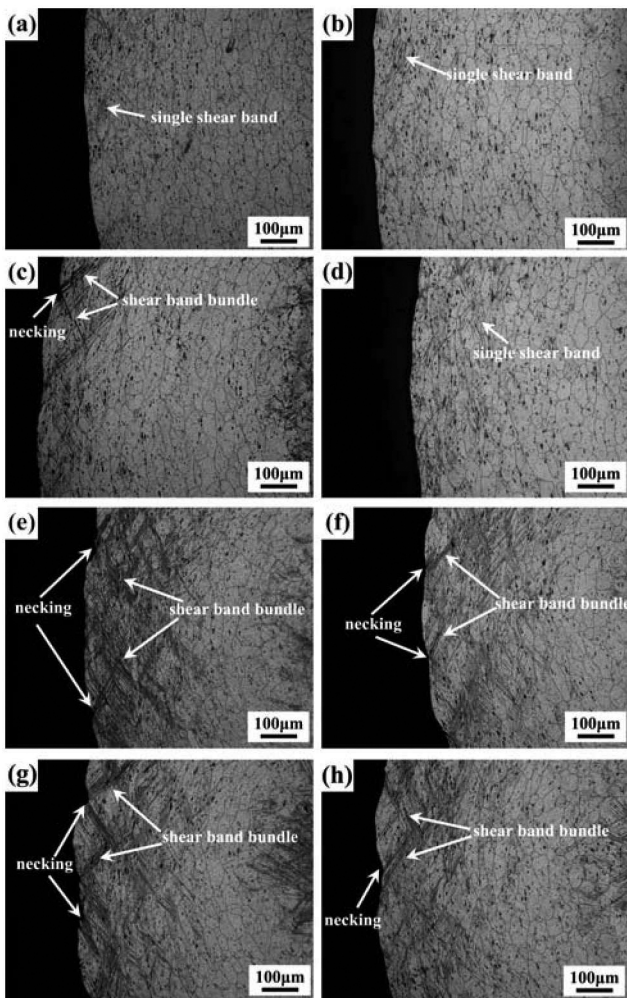


Figure 6. Cross sections of the specimens after bending to different angles: (a) RD, 60°, (b) TD, 60°, (c) RD, 90°, (d) TD, 90°, (e) RD, 120°, (f) TD, 120°, (g) RD, 150°, (h) TD, 150°

The results of Takeda et al. [10] and Ikawa et al. [11] suggested that, for single-crystal specimens with cube orientation, less shear band would form after 180° bending regardless of bending direction. However, for the specimens with $Goss_{ND90}$, R,

P, and Cu orientations, shear bands would form prior in RD specimens, while for Goss specimens, shear bands would form preferentially in TD specimens. For single-crystal specimens, the shear bands are usually initiated at the surface. In the present study, when the specimens were bent to 60°, some shear band formed in some grains with special orientation underlying the surface, such as the grains with $Goss_{ND90}$, R, P, and Cu orientations in RD specimen and the grains with Goss orientation. With the increase of the bending angle, more shear bands would form, and the shear bands in the adjoining grains merged, resulting in the formation of shear band bundles. Table II shows that the total volume fraction of $Goss_{ND90}$, R, P, and Cu orientations is almost twice as that of Goss orientation. Thus the formation and propagation of shear bands would be facilitated in the RD specimens. Two bundles of shear bands intersect at the surface caused strain localization, resulting in the forming of necking. Thus, RD specimen exhibits inferior bendability compared with TD specimen.

Furthermore, it is interesting to note that although some severe strain localizations were induced in the RD and TD 180° bending specimens, no macro-crack were formed. Figure 7 shows that some constitute particles had cracked and some micro-voids formed after 180° bending. However, the micro-crack and voids did not propagate along the shear band, indicating the high crack propagation resistance of the 6016-T4P sheet.

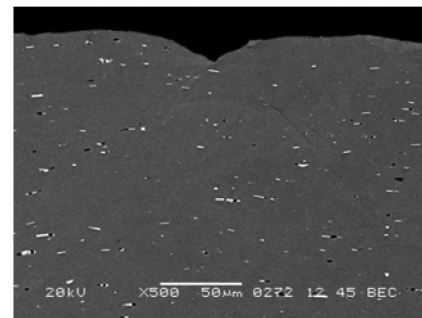


Figure 7. SEM images of the cross section of RD specimen after 180° bending showing the crack of constitute particles

Conclusions

In the present study, the bending performance in RD and TD directions of an AA6016-T4P automotive sheet was investigated. The following conclusions were drawn.

- 1) No macro-crack formed in both RD and TD specimens after 180° bending. However, RD specimen exhibited inferior bendability compared with TD specimen, showing more severe surface necking in the RD specimen.
- 2) The anisotropy of surface necking in the AA6016-T4P sheet was caused by special crystallographic texture, rather than grain shape and spatial distribution of the constitute particles.
- 3) The total volume fraction of $Goss_{ND90}$, R, P, and Cu orientations was almost twice as that of Goss orientation in the AA6016-T4P sheet, resulting in the facilitation of the initiation and propagation of shear bands in the RD specimens, and then leading to more severe surface necking

Acknowledgments

The authors gratefully acknowledge the support of the National High-tech R&D Program (863 Program) of China under Grant No. 2013AA032403

References

- [1] W.S. Miller, L. Zhuang, J. Bottema, A.J. Wittebrood, P. D. Smet, A. Haszler and A. Vieregge, "Recent development in aluminum alloys for the automotive industry," *Materials Science and Engineering A*, 280 (2000), 37-49.
- [2] Y. Muraoka and H. Miyaoka, "Development of an all-aluminum automotive body," *Journal of Materials Processing Technology*, 38 (1993), 655-674.
- [3] G.S. Cole and A.M. Sherman, "Light weight materials for automotive application," *Materials. Characterization*, 35 (1995), 3-9.
- [4] O. Engler and J. Hirsch, "Texture control by thermomechanical processing of AA6xxx Al-Mg-Si sheet alloys for automotive application-a review," *Materials Science and Engineering A*, 336 (2003), 249-262.
- [5] O. Engler, C. Schäfer and H.J. Brinkman, "Crystal-plasticity simulation of the correlation between microtexture and roping in an AA6xxx Al-Mg-Si sheet alloys for automotive application," *Acta Materialia*, 60 (2012), 5217-5232.
- [6] P. Jimbert, I. Eguiaa, I. Perez, M.A. Gutierrez and I. Hurtado, "Analysis and comparative study of factors affecting quality in the hemming of AA6016-T4 performed by means of electromagnetic forming and process characterization," *Journal of Materials Processing Technology*, 211 (2011), 916-924.
- [7] M. Asano, T. Minoda, Y. Ozeki and H. Yoshida, "Effect of copper content on the bendability of Al-Mg-Si alloy sheet," *Materials Science Forum*, 519-521 (2006), 771-776.
- [8] I. Westerman, K.E. Snilsberg, Z. Sharifi, O.S. Hopperstad, K. Marthinsen and B. Holmedal, "Three-point bending of heat-treatable aluminum alloys: influence of microstructure and texture on bendability and fracture behavior," *Metallurgical and Materials Transactions A*, 42 (2011), 3386-3398.
- [9] A. Davidkov, R.H. Petrov, P.D. Smet, B. Schepers and L.A.I. Kestens, "Microstructure controlled bending response in AA6016 Al alloys," *Materials Science and Engineering A*, 528 (2011), 7068-7076.
- [10] H. Takeda, A. Hibino and K. Takata, "Influence of crystal orientation on the bendability of an Al-Mg-Si alloy," *Materials Transactions*, 51 (2010), 614-619.
- [11] S. Ikawa, M. Asano, M. Kuroda and K. Yoshida, "Effects of crystal orientation on bendability of aluminum alloy sheet," *Materials Science and Engineering A*, 528 (2011), 4050-4054.
- [12] M. Kuroda and V. Tvergaard, "Effects of texture on shear band formation in plane strain tension/compression and bending," *International Journal of Plasticity*, 23 (2007), 244-272.
- [13] Y. Shi, H. Jin, P.D. Wu, D.J. Lloyd and D. Embury, "Failure analysis of fusion clad alloy system AA3003/AA6xxx sheet under bending," *Materials Science and Engineering A*, 610 (2014), 263-272.
- [14] L. Mattei, D. Daniel, G. Guiglionda, H. Klöcker and J. Driver, "Strain localization and damage mechanisms during bending of AA6016 sheet," *Materials Science and Engineering A*, 559 (2013), 812-821.
- [15] ASTM Standard E290, "Standard Test Methods for Bend Testing of Material for Ductility," ASTM International, West Conshohocken, PA, 2004.
- [16] H. Zhong, P.A. Rometsch and Y. Estrin, "The influence of Si and Mg content on the microstructure, tensile ductility, and stretch formability of 6xxx alloys," *Metallurgical and Materials Transactions A*, 44 (2013), 3970-3983.
- [17] J. Sidor, R.H. Petrova and L.A.I. Kestens, "Deformation, recrystallization and plastic anisotropy of asymmetrically rolled aluminum sheets," *Materials Science and Engineering A*, 528 (2010), 413-424.